A New Series of Oxygen-Deficient Perovskites in the $NaTi_xNb_{1-x}O_{3-0.5x}$ System: Synthesis, Crystal Chemistry, and Energetics

Hongwu Xu,*,† Yali Su,‡ M. Lou Balmer,‡,§ and Alexandra Navrotsky†

Thermochemistry Facility and NEAT ORU, University of California at Davis, Davis, California 95616, and Pacific Northwest National Laboratory, P.O. Box 999, MSIN K8-93, Battelle Boulevard, Richland, Washington 99352

Received September 24, 2002. Revised Manuscript Received February 20, 2003

A series of perovskites with the compositions $NaTi_xNb_{1-x}O_{3-0.5x}$ ($0 \le x \le 0.2$) has been synthesized for the first time using the sol−gel method. Combined Rietveld analysis of powder neutron and X-ray diffraction data reveals that these phases adopt the structure of the end-member perovskite $NaNbO_3$ with the space group *Pbma*. However, the substituted structure is deficient in oxygen over its O1 and O3 sites, which compensates the charge imbalance between the substituting Ti^{4+} and Nb^{5+}. Raman spectroscopy indicates that the O^{2-} vacancies are locally associated with Ti^{4+}, resulting in $[TiO_5]$ coordination. There is no evidence for long-range order or superstructure. With increasing Ti content, the orthorhombic structure becomes more like the cubic, as reflected by the smaller differences among its cell parameters (a_p, b_p, and c_p) and the cell angle β_p approaching 90° (in terms of the pseudocubic subcell). Enthalpies of formation from the oxides and from the elements have been determined by drop solution calorimetry into molten $3Na_2O{\cdot}4MoO_3$ solvent at 974 K. As Ti^{4+} substitutes for Nb^{5+}, the formation enthalpies become less exothermic, suggesting a destabilizing effect of the substitution. We attribute this behavior to a number of structural factors, including the occurrence of O^{2-} vacancies and of Ti−O−Nb linkages as well as the size mismatch between Ti^{4+} and Nb^{5+}.

Introduction

Sodium niobate ($NaNbO_3$) and its related perovskites have attracted considerable attention due to their unique combination of superior electrical and mechanical properties.[1−3] Since they are lead-free, these phases are environmentally more benign than lead-based ferroelectric materails. In addition, this group of materials is of interest from the crystal-chemical viewpoint because they exhibit a rich variety of thermally induced phase transitions.

Like other ABO_3 perovskites, $NaNbO_3$ comprises a three-dimensional framework of corner-sharing $[BO_6]$ ($[NbO_6]$ for $NaNbO_3$) octahedra with A cations (Na in $NaNbO_3$) occupying its cavities (Figure 1). The room-temperature structure of $NaNbO_3$ has long been treated as orthorhombic with the space group *Pbma* or *Pbcm* (depending on the choice of unit-cell setting),[4,5] although a recent neutron diffraction study presents evidence for a lower symmetry.[6] On heating, $NaNbO_3$ undergoes a sequence of displacive transitions to phases with higher symmetries and eventually transforms to the ideal cubic structure (*Pm*3*m*) at ∼914 K.[7−10] In addition, there exists a low-temperature transformation to the rhombohedral phase (*R*3*c*) at ∼163 K.[11] These structural

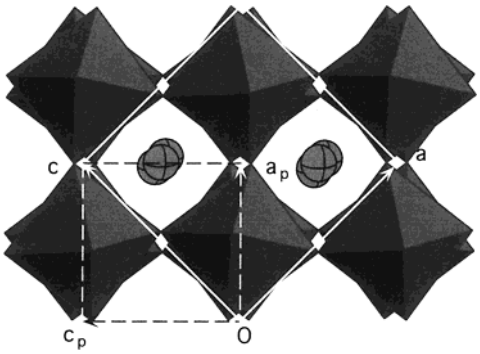

Figure 1. Crystal structure of $NaNbO_3$ perovskite projected down [010]. Octahedra represent $[NbO_6]$ units, and spheres represent Na ions. Solid lines outline the unit cell and dashed lines the pseudocubic subcell.

* To whom correspondence should be addressed.
† University of California at Davis.
‡ Pacific Northwest National Laboratory.
§ Present address: Caterpillar Inc., Technical Center, E/854, P.O. Box 1875, Peoria, IL 61656.

(1) Reznitchenko, L. A.; Dergunova, N. V.; Geguzina, G. A.; Razumovskaya, O. N.; Shilkina, L. A.; Ivanova, L. S. *Ferroelectrics* **1998**, *214*, 241.
(2) Geguzina, G. A.; Reznitchenko, L. A.; Dergunova, N. V. *Ferroelectrics* **1998**, *214*, 261.
(3) Reznitchenko, L. A.; Turik, A. V.; Kuznetsova, E. M.; Sakhnenko, V. P.; *J. Phys.: Condens. Matter* **2001**, *13*, 3875.
(4) Sakowski-Cowley, A. C.; Lukaszewicz, K.; Megaw, H. D. *Acta Crystallogr.* **1969**, *B25*, 851.
(5) Hewat, A. W. *Ferroelectrics* **1974**, *7*, 83.
(6) Darlington, C. N. W.; Knight, K. S. *Physica* **1999**, *B266*, 368.
(7) Ahtee, M.; Glazer, A. M.; Megaw, H. D. *Philos. Mag.* **1972**, *26*, 995.
(8) Glazer, A. M.; Megaw, H. D. *Philos. Mag.* **1972**, *25*, 1119.
(9) Darlington, C. N. W.; Knight, K. S. *Acta Crystallogr.* **1999**, *B55*, 24.
(10) Glazer, A. M.; Megaw, H. D. *Acta Crystallogr.* **1973**, *A29*, 489.

10.1021/cm020963s CCC: $25.00
Published on Web 04/08/2003

transitions in $NaNbO_3$ result in changes in electrical properties from ferroelectric to antiferroelectric and then to paraelectric with increasing temperature.[12]

The rich polymorphism in $NaNbO_3$ largely arises from the ease of twisting its framework by tilting $[NbO_6]$ octahedra about the ⟨100⟩ axes. Thus, one suspects that this structure is also tolerant of ionic substitutions. $NaNbO_3$-based solid solutions have been synthesized, though in some cases with limited solubility, in many systems.[1] They fall into two categories. In one, Na^+ is replaced by other cations such as Li^+, Mg^{2+}, and Mn^{2+}. Charge compensation, if necessary, occurs by A-site vacancies. In the other, the charge-coupled substitutions involve both A- and B-cations (e.g., $Sr^{2+} + Ti^{4+} \rightarrow Na^+ + Nb^{5+}$). These solid solutions exhibit systematic changes in structure and physical properties (such as ferroelectric permittivity) as a function of composition.[1,2] Therefore, their properties can be tailored for specific applications by varying their dopant contents.

The present work reports a new series of $NaNbO_3$-based solid solutions, $NaTi_xNb_{1-x}O_{3-0.5x}$ ($0 \leq x \leq 0.2$). In this series, a portion of the Nb^{5+} is replaced by Ti^{4+}, and the charge is balanced by the creation of O^{2-} vacancies. Our motivation for this study is 2-fold. First, these phases are present as major components in a potential ceramic waste form for radioactive ^{137}Cs or ^{90}Sr. Specifically, IE-911, an engineered form of crystalline silicotitanate (CST) ion exchanger, has been proposed to be used for separating ^{137}Cs from Na-rich waste streams because of its high selectivity for Cs^+ over Na^+.[13] Similarly, a recently synthesized series of niobate-based microporous materials, $NaTi_xNb_{2-x}O_{6-x}(OH)_x \cdot H_2O$, exhibits high selectivity for Sr^{2+},[14,15] and thus can potentially be used for ^{90}Sr extraction. Calcination of the Cs− or Sr-loaded ion exchanger into a thermally stable and chemically durable ceramic waste form is a proposed strategy.[13] These perovskite phases appear on calcination. To assess the feasibility of this disposal plan, a thorough understanding of the structures and thermodynamic stability for all the components, including the $NaNbO_3$-based perovskite phases, in the waste form is essential. Second, as in other doped perovskites (such as Sr/Mg-doped $LaGaO_3$),[16] the vacancies in $NaTi_xNb_{1-x}O_{3-0.5x}$ may serve as the energetically favorable sites for O^{2-} diffusion, thereby possibly rendering these materials high ionic conductivity.

In this study, a suite of $NaTi_xNb_{1-x}O_{3-0.5x}$ ($0 \leq x \leq 0.2$) perovskites was synthesized by the sol−gel method. Combined Rietveld analysis of powder neutron and X-ray diffraction data allows high-resolution determination of their unit-cell parameters, atomic positions, and atomic thermal parameters. Raman spectroscopy was performed to reveal the Ti/Nb−O bonding configurations on a more local scale. The enthalpies of formation from the constituent oxides and from the elements were measured using high-temperature drop solution calorimetry. Trends in the formation enthalpies as a function of Ti/(Ti + Nb) are then discussed in terms of the crystal chemistry.

Experimental Techniques

Sample Synthesis. Five samples with the compositions $NaTi_xNb_{1-x}O_{3-0.5x}$, $x = 0$, 0.05, 0.1, 0.15, and 0.2, were synthesized via a sol−gel processing route. First, an amorphous, homogeneous precursor for each composition was prepared using niobium ethoxide (NbEO), titanium isopropoxide (TIP), and sodium hydroxide. The alkoxides (NbEO and TIP) with the desired ratio were mixed in a reaction flask in a glovebox under an Ar atmosphere, and the flask was sealed with a rubber stopper and transferred to a stir plate. A solution of NaOH (50 wt %) and ethanol was then injected into the alkoxide mixture using a syringe, followed by the injection of an equal volume of ethanol. This process was repeated several times with intervals of 15 min until the desired Na:Nb:Ti ratio was achieved. After gelation, additional water and ethanol were added to dissolve the gel, and the liquid was then stirred and dried in air overnight. Second, ∼0.5 g of the obtained precursor was ground, pressed into pellets, and then heat-treated in air at 1173 K for ∼15 h. Thermogravimetric analysis (TGA) indicates that the gel precursor lost its molecular water up to 673 K and then lost its hydroxyl around 1073 K, with no weight change above 1173 K. The final product was a white, monophasic crystalline material, as revealed by X-ray and neutron diffraction (see below).

Powder Neutron and X-ray Diffraction. Powder diffraction experiments were performed with both time-of-flight neutron and laboratory X-ray radiation. Neutron measurements were carried out using the high-pressure preferred orientation (HIPPO) diffractometer at the Manuel Lujan, Jr. Neutron Scattering Center of the Los Alamos National Laboratory. Sample powders for each composition were filled into a vanadium can ∼0.7 cm in diameter, and the can was fully rotated during data collection. Data were simultaneously collected in four detector banks centered at ±90° and ±151° 2θ.

Conventional X-ray diffraction was conducted with a Scintag Pad-V diffractometer using Cu Kα radiation. Sample powders were mounted in a front-loading, shallow-cavity zero-background quartz holder, and data were collected from 5° to 120° 2θ in step scan mode using steps of 0.02° with a counting time of 10 s.

The Rietveld method[17] was used to analyze the neutron and X-ray data simultaneously with the General Structure Analysis System (GSAS) program of Larson and Von Dreele.[18] The starting atomic parameters of the end-member perovskite $NaNbO_3$ were taken from the study of Sakowski-Cowley et al.[4] We then used our refined structural parameters of $NaNbO_3$ as the starting parameters for the next-nearest composition ($x = 0.05$) and continued this procedure systematically with increasing Ti content. The refinements proceeded as follows: After the scale factor and four background terms had converged, specimen displacement and lattice parameters were added and optimized. Between five and eight additional background terms were then added for each histogram, and the peak profiles were fitted to pseudo-Voigt functions with a peak asymmetry correction.[19,20] On convergence of the preceding parameters, atomic coordinates and isotropic temperature

(11) Darlington, C. N. W.; Megaw, H. D. *Acta Crystallogr.* **1973**, *B29*, 2171.
(12) Lines, M. E.; Glass, A. M. *Principles and Applications of Ferroelectrics and Related Materials*; Clarendon Press: Oxford, 1977.
(13) Su, Y.; Balmer, M. L.; Wang, L.; Bunker, B. C.; Nyman, M.; Nenoff, T.; Navrotsky, A. In *Scientific Basis for Nuclear Waste Management XXII*; Wronkiewicz, D. J., Lee, J. H., Eds.; Materials Research Society Symposium Proceedings 556; MRS: Pittsburgh, PA, 1999; pp 77−84.
(14) Nyman, M.; Tripathi, A.; Parise, J. B.; Maxwell, R. S.; Harrison, W. T. A.; Nenoff, T. M. *J. Am. Chem. Soc.* **2001**, *123*, 1529.
(15) Nyman, M.; Tripathi, A.; Parise, J. B.; Maxwell, R. S.; Nenoff, T. M. *J. Am. Chem. Soc.* **2002**, *124*, 1704.
(16) Huang, K.; Tichy, R. S.; Goodenough, J. B. *J. Am. Ceram. Soc.* **1998**, *81*, 2565.
(17) Rietveld, H. M. *J. Appl. Crystallogr.* **1969**, *2*, 65.
(18) Larson A. C.; Von Dreele, R. B. *GSAS−General Structure Analysis System*; Los Alamos National Laboratory Report No. LAUR 86-748; Los Alamos National Laboratory: Los Alamos, NM, 2000.
(19) Thompson, P.; Cox, D. E.; Hastings, J. *J. Appl. Crystallogr.* **1987**, *20*, 79.

Table 1. Unit-Cell Dimensions and Refinement Agreement Parameters of $NaTi_xNb_{1-x}O_{3-0.5x}$ Perovskites

x	a (Å)	b (Å)	c (Å)	V (Å^3)	R_{wp} (%)	R_p (%)
0	5.5625(4)	15.5495(10)	5.5138(4)	476.91(8)	4.6	2.8
0.05	5.5528(5)	15.5597(11)	5.5140(5)	476.40(9)	4.6	2.8
0.1	5.5428(5)	15.5632(11)	5.5094(5)	475.26(8)	4.6	3.0
0.15	5.5396(4)	15.5705(11)	5.5087(4)	475.14(5)	4.7	3.0
0.2	5.5303(4)	15.5677(12)	5.5072(4)	474.14(5)	5.5	3.2

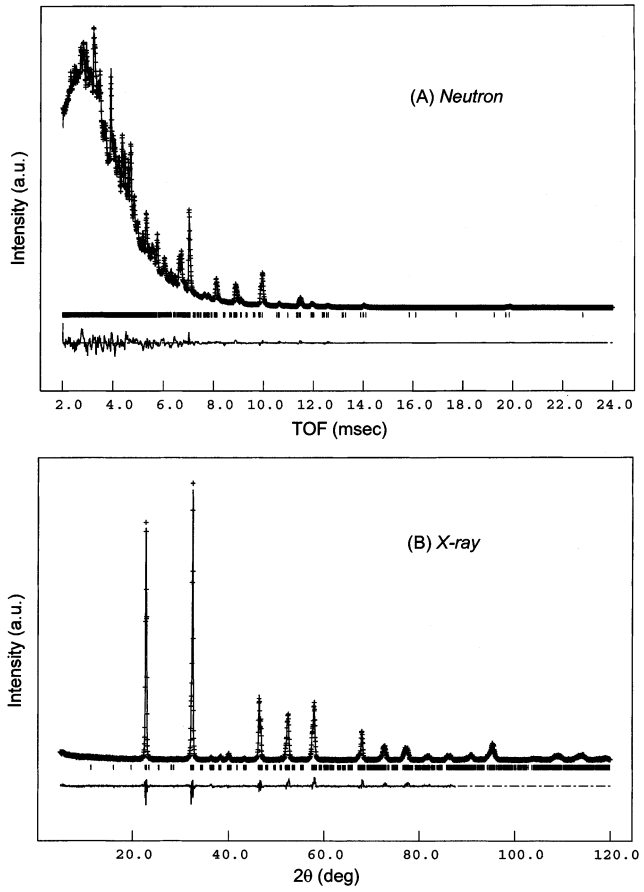

Figure 2. Representative (A) neutron and (B) X-ray diffraction patterns ($NaNbO_3$) fitted using the Rietveld method. Data are shown by plus signs, and the solid curves are the best fits to the data from the combined refinement. Tick marks below each pattern show the positions of allowed reflections, and the lower curve represents the difference between the observed and calculated profiles.

factors for Na, Nb/Ti, and O were refined, yielding R_{wp} values ranging from 4.6% to 5.5% (Table 1). A representative pair of fitted patterns is plotted in Figure 2.

Raman Spectroscopy. Raman spectroscopic experiments were conducted using a Spex Triple Raman Spectrometer (Industries model 1977) with the 488-nm line of a Coherent Innova 307 Ar^+ ion laser for excitation. The power at the sample was on the order of 100 mW. A LN/CCD detector (Princeton Instruments) was used with a typical exposure time of 10 s and a slit width of 100 μm. Sample powders for each composition were pressed into a pellet, and its Raman spectrum was collected at the 180° scattering geometry. Peak positions were calibrated against the known bands of aspirin with an accuracy of ~1 cm^{-1}.

High-Temperature Drop Solution Calorimetry. High-temperature calorimetric measurements were performed using a custom-built Tian-Calvet microcalorimeter operating at 974 K with molten sodium molybdate ($3Na_2O{\cdot}4MoO_3$) as the solvent. The equipment and experimental procedure have been described in detail by Navrotsky.[21] A sample pellet weighing ~5 mg was dropped from room temperature into the solvent in the hot calorimeter. The heat effect measured includes the energy associated with heating the sample from room temperature to 974 K (heat content) plus the enthalpy of solution of the sample. The calorimeter was calibrated against the known heat content of ~5-mg corundum pellets. Between 5 and 12 sample pellets were dropped for each composition. To ensure there is no surface water, which would have a significant endothermic effect, present in samples, all the samples were dried at ~403 K overnight immediately before the calorimetric experiments.

Table 2. Atomic Coordinates and Isotropic Temperature Factors of $NaTi_xNb_{1-x}O_{3-0.5x}$ Perovskites (Space Group *Pbma*)[a]

x:	0	0.05	0.1	0.15	0.2
Na1(z)	0.234(2)	0.230(4)	0.244(1)	0.238(1)	0.242(2)
Na2(x)	0.743(2)	0.742(3)	0.746(2)	0.744(2)	0.745(3)
Na2(z)	0.240(2)	0.248(4)	0.256(1)	0.254(2)	0.256(2)
Nb/Ti(x)	0.2583(4)	0.2598(5)	0.2612(5)	0.2602(6)	0.2602(6)
Nb/Ti(y)	0.1260(2)	0.1267(2)	0.1253(2)	0.1252(2)	0.1257(3)
Nb/Ti(z)	0.2462(5)	0.2415(5)	0.2390(3)	0.2377(3)	0.2394(4)
O1(z)	0.3110(8)	0.2944(10)	0.2752(8)	0.2688(8)	0.2673(12)
O2(x)	0.2402(12)	0.2485(16)	0.2533(13)	0.2518(15)	0.2516(20)
O2(z)	0.1817(8)	0.1796(9)	0.1735(9)	0.1715(9)	0.1724(12)
O3(x)	0.0679(5)	0.0699(6)	0.0612(5)	0.0570(6)	0.0555(8)
O3(y)	0.1397(2)	0.1387(2)	0.1373(2)	0.1370(2)	0.1366(3)
O3(z)	0.5443(6)	0.5433(7)	0.5401(8)	0.5384(8)	0.5390(11)
O4(x)	0.4919(8)	0.4948(10)	0.4945(9)	0.4909(9)	0.4890(12)
O4(y)	0.1102(2)	0.1090(2)	0.1065(2)	0.1072(2)	0.1077(2)
O4(z)	−0.0119(8)	−0.0176(8)	−0.0234(9)	−0.0242(9)	−0.0254(12)
U(Na)[b]	1.49(5)	1.65(7)	0.74(6)	0.90(6)	1.40(8)
U(Nb/Ti)[b]	0.40(2)	0.45(2)	0.47(2)	0.30(2)	0.58(2)
U(O)[b]	0.69(2)	0.69(2)	0.66(2)	0.74(2)	0.87(3)

[a] The x and y coordinates of Na1 are 0.75 and 0, respectively; the y coordinate of Na2 is 0.25; the x and y coordinates of O1 are 0.25 and 0, respectively; and the y coordinate of O2 is 0.25. [b] The thermal parameters of like atoms are constrained to be equal. Unit: Å^2/100.

Results and Discussion

Crystal Structure. Rietveld analyses of our neutron and X-ray data indicate that all the $NaTi_xNb_{1-x}O_{3-0.5x}$ ($0 \le x \le 0.2$) perovskites adopt the $NaNbO_3$ structure with the space group *Pbma* (Figure 1). Although a recent high-resolution neutron diffraction study of $NaNbO_3$ argues that its structure may be monoclinic,[6] close inspection of our own diffraction patterns reveals no peak splittings, indicative of a lower symmetry. Moreover, the Ti-substituted phases exhibit neither extra reflections nor absence of certain reflections that would suggest space groups other than *Pbma*. In the Ti-substituted structure, Ti occupies the same type of sites as Nb. However, the O vacancies, which compensate the charge imbalance between Ti^{4+} and Nb^{5+}, appear to occur over half the available sites. Specifically, among the four types of O positions, O1 and O3 are deficient in oxygen, whereas O2 and O4 are fully occupied (see below for further discussion). The refined lattice parameters, atomic coordinates, and isotropic temperature factors are listed in Tables 1 and 2.

Figure 3 shows unit-cell parameters of $NaTi_xNb_{1-x}O_{3-0.5x}$ perovskites as a function of composition. For ease of comparison, cell parameters (a, b, and c) are expressed in terms of the pseudocubic subcell [a_p, b_p, c_p ($=a_p$), and β_p]: $a = 2a_p \sin(\beta_p/2)$; $b = 4b_p$; $c = 2a_p \cos(\beta_p/2)$ (Figure 1). With increasing Ti content,

(20) Finger, L. W.; Cox, D. E.; Jephcoat, A. P. *J. Appl. Crystallogr.* **1994**, *27*, 892.

(21) Navrotsky, A. *Phys. Chem. Miner.* **1997**, *24*, 222.

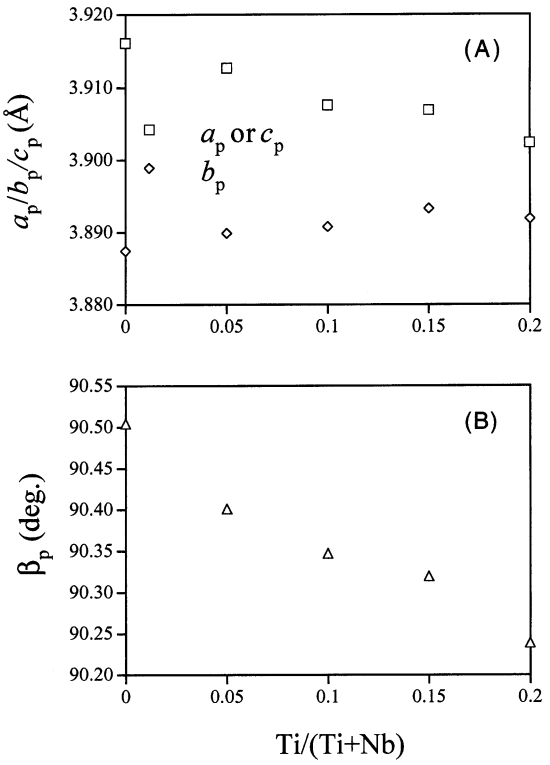

Figure 3. Variation of cell parameters (A) a_p, b_p, c_p and (B) β_p in terms of the pseudocubic subcell for $NaTi_xNb_{1-x}O_{3-0.5x}$ perovskites as a function of composition. Errors are smaller than the size of symbols.

cell parameters a_p and c_p ($a_p = c_p$) decrease, whereas b_p slightly increases (Figure 3A). As a result, cell volume decreases. This trend is consistent with the replacement of Nb^{5+} (ionic radius = 0.64 Å in 6-coordination[22]) by the smaller Ti^{4+} (0.605 Å in 6-coordination[22]). Although the occurrence of O^{2-} vacancies may cause lattice expansion, as seen in some other oxygen-deficient perovskites,[23−25] this effect is obviously smaller than that due to the Ti → Nb substitution. Further, as Ti/(Ti + Nb) increases, the difference between a_p and b_p becomes smaller, and the cell angle β_p closer to 90° (Figure 3), suggesting that the structure becomes more like the cubic. This behavior can be explained in terms of the tolerance factor (t) for ABO_3 perovskites: $t = (r_A + r_O)/\sqrt{2}(r_B + r_O)$, where r_A, r_B, and r_O refer to the ionic radius of A, B, and O^{2-}, respectively. In the ideal cubic perovskite structure, the ratio of the A−O bond length ($r_A + r_O$) to the B−O length ($r_B + r_O$) equals $\sqrt{2}$, and thus $t = 1$. When this condition cannot be met, the structure distorts.[26] In orthorhombic $NaNbO_3$ ($t \approx 0.94$, calculated based on the bond lengths from ref 4 and assuming Na is 8- or 9-fold coordinated), the Nb−O bond is longer than needed to match the Na−O bond to form an ideal cubic structure. With increasing Ti → Nb substitution, however, the mean bond length ⟨B−O⟩ (B = Nb, Ti) decreases (Figure 4), and thus the tolerance factor t becomes closer to unity. In other words, the deviation of the structure from the ideal cubic symmetry decreases with increasing Ti substitution.

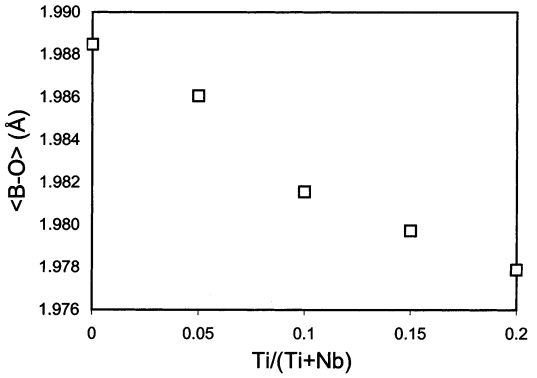

Figure 4. Variation of the mean bond length ⟨B−O⟩ (B = Nb or Ti) of $NaTi_xNb_{1-x}O_{3-0.5x}$ perovskites as a function of composition. Errors are smaller than the size of the symbol.

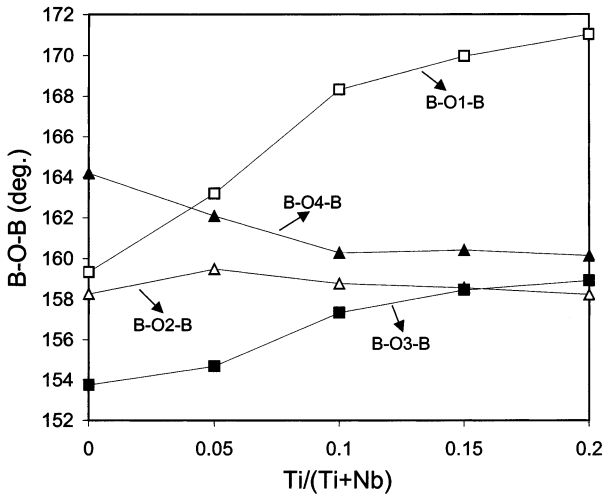

Figure 5. Variation of bond angles B−O1−B (B = Nb or Ti), B−O2−B, B−O3−B, and B−O4−B of $NaTi_xNb_{1-x}O_{3-0.5x}$ perovskites as a function of composition. Errors are smaller than the size of symbols.

As described earlier, on heating, $NaNbO_3$ undergoes a sequence of displacive transitions before it becomes cubic at ~914 K. These transitions occur largely through the tilting of [NbO_6] octahedra in the framework. Likewise, the structural variations induced by Ti → Nb substitution also result from octahedral framework distortion, as is reflected in the systematic changes in B−O−B bond angles as a function of composition. With increasing Ti/(Ti + Nb), the bond angles B−O1−B and B−O3−B, which are associated with the O positions (O1 and O3) over which the vacancies occur, increase and B−O2−B remains approximately constant, whereas B−O4−B decreases (Figure 5). Since the B−O1−B−O2−B zigzag chains run parallel to the $\mathbf{b_p}$ axis, and since the layers comprised of these chains are perpendicular to $\mathbf{[101]_p}$ (Figure 6A), increasing the B−O1−B angle lengthens the b_p-dimension while shortening a_p and c_p ($=a_p$). Similarly, as the layers consisting of B−O3−B−O4−B linkages are parallel to (010) (Figure 6B), reducing the difference between B−O3−B and B−O4−B decreases the β_p angle, which becomes closer to 90°. Correspondingly, the structure becomes more cubiclike.

Although $NaTi_xNb_{1-x}O_{3-0.5x}$ perovskites exhibit systematic structural variations toward the cubic phase

(22) Shannon, R. D. *Acta Crystallogr.* **1976**, *A32*, 751.
(23) Armstrong, T. R.; Stevenson, J. W.; Pederson, L. R.; Raney, P. E. *J. Electrochem. Soc.* **1996**, *143*, 2919.
(24) Yang, J. B.; Yelon, W. B.; James, W. J.; Chu, Z.; Kornecki, M.; Xie, Y. X.; Zhou, X. D.; Anderson, H. U.; Joshi, A. G.; Malik, S. K. *Phys. Rev. B: Condens. Matter Mater. Phys.* **2002**, *66*, 184415.
(25) Ullmann, H.; Trofimenko, N. *J. Alloys Compd.* **2001**, *316*, 153.
(26) Navrotsky, A. *Chem. Mater.* **1998**, *10*, 2787.

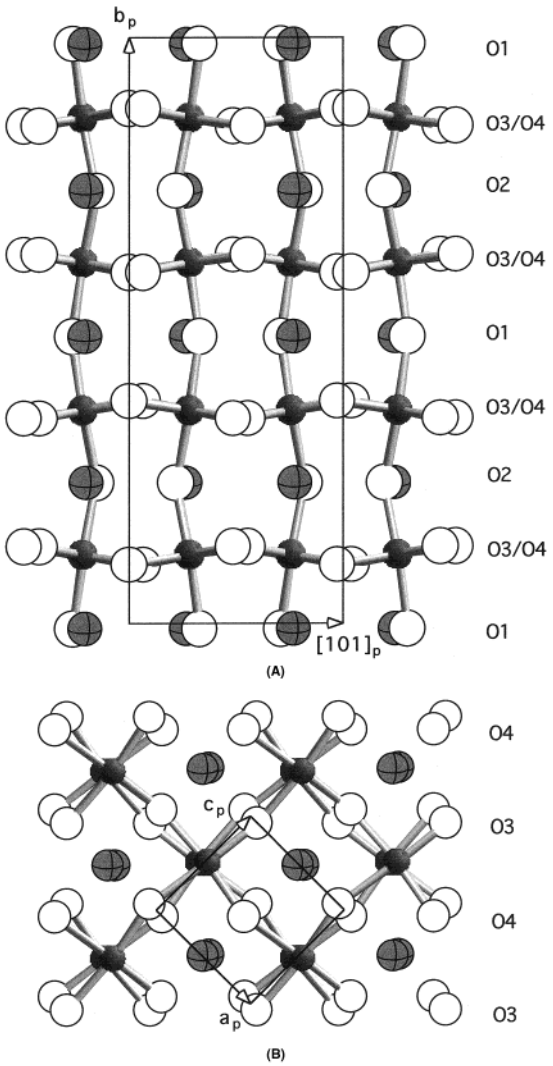

Figure 6. Structural projections of $NaTi_xNb_{1-x}O_{3-0.5x}$ perovskite along (A) [100] (or $[10\bar{1}]_p$) and (B) [010] (or $[010]_p$). Solid spheres represent B cations (B = Nb or Ti), filled equatorials represent Na ions, and circles represent O atoms. Thin lines outline the pseudocubic subcell. For clarity, atoms in a partial subcell along the projection axis are shown.

with increasing Ti content, we find no evidence for phase transitions that are analogous to those in $NaNbO_3$ at elevated temperatures. This may be because the extent of Ti → Nb substitution achieved ($x \leq 0.2$) is not large enough to induce any symmetry changes. In fact, the room-temperature phase of $NaNbO_3$ exists over a large temperature range (163−646 K),[10,11] and thus this structure can probably be stable up to a relatively high amount of Ti substitution at room temperature. However, as the reflections that distinguish the different orthorhombic polymorphs in $NaNbO_3$ tend to be very weak and as the resolutions of our neutron/X-ray data may not be high enough to reveal them, we cannot rule out the possibility that the Ti-substituted phases adopt a slightly different structure(s). To obtain a more decisive conclusion, experimental techniques that are better suited for revealing weak reflections (such as electron diffraction coupled with high-resolution transmission electron microscopy imaging) need to be employed.

Framework Cation Local Ordering. Although Nb and Ti occupy the same type of sites in the

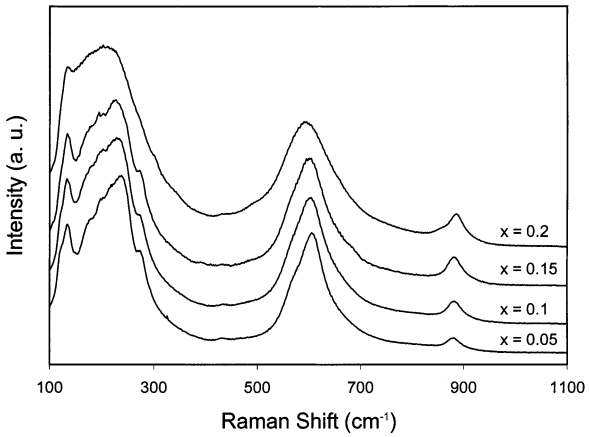

Figure 7. Raman spectra of $NaTi_xNb_{1-x}O_{3-0.5x}$ perovskites.

$NaTi_xNb_{1-x}O_{3-0.5x}$ structure, which precludes any long-range Nb/Ti order, they may have different local bonding environments and thus be ordered on a local scale. Figure 7 shows Raman spectra of $NaTi_xNb_{1-x}O_{3-0.5x}$ perovskites. As demonstrated in previous Raman studies of $NaNbO_3$ perovskite,[27−29] the bands in the region 100−700 cm^{-1} are related to the internal modes of $[NbO_6]$. The bands due to the translational modes of Na^+ and the librational modes of $[NbO_6]$ are at <100 cm^{-1},[27−29] which were not measured in our experiments. A new band at ~880 cm^{-1} appears for the Ti-substituted phases, and further, its intensity increases with increasing Ti content. As observed in many silicotitanates whose Raman bands at 800−950 cm^{-1} are generally due to the $[TiO_5]$ coordination,[30] this band can be assigned to the Ti−O stretch in $[TiO_5]$. Hence, in the Ti-substituted structure, each Ti is bonded to five oxygen atoms, forming a $[TiO_5]$ square pyramid, as compared with the 6-fold coordination for Nb.

The occurrence of $[TiO_5]$ in the $NaTi_xNb_{1-x}O_{3-0.5x}$ structure dictates that the O vacancies, which compensate the charge imbalance between Ti^{4+} and Nb^{5+}, are mainly associated with Ti. Furthermore, to maintain the octahedral coordination for Nb, the $[TiO_5]$ pyramids must occur in pairs, with the square bases of the paired $[TiO_5]$ being next to each other. The resulting $[Ti_2O_{10}]$ unit is then linked to $[NbO_6]$ octahedra through corner-sharing. The next-nearest neighbors for the $[Ti_2O_{10}]$ unit could be either $[Ti_2O_{10}]$ or $[NbO_6]$, depending on the composition and synthesis conditions of the sample. Therefore, on a short-range scale, neither Ti/Nb nor O vacancies are randomly distributed. Rather, they are ordered and their locations are strongly correlated. The charge-coupled substitution, $Ti^{4+} + 0.5V_O^{\bullet\bullet} = Nb^{5+}$, and the induced local structural changes are thus quite unique.

Thermochemistry. The heats of drop solution (ΔH_{ds}) of $NaTi_xNb_{1-x}O_{3-0.5x}$ perovskites in molten $3Na_2O\cdot 4MoO_3$ at 974 K are presented in Table 3 and Figure 8A. Using these data and the reported ΔH_{ds} values for

(27) Wang, X. B.; Shen, Z. X.; Hu, Z. P.; Qin, L.; Tang, S. H.; Kuok, M. H. *J. Mol. Struct.* **1996**, *385*, 1.
(28) Shen, Z. X.; Wang, X. B.; Kuok, M. H.; Tang, S. H. *J. Raman Spectrosc.* **1998**, *29*, 379.
(29) Shen, Z. X.; Wang, X. B.; Tang, S. H.; Kuok, M. H.; Malekfar, R. *J. Raman Spectrosc.* **2000**, *31*, 439.
(30) Su, Y.; Balmer, M. L.; Bunker, B. C. *J. Phys. Chem. B* **2000**, *104*, 8160.

Table 3. Enthalpies of Drop Solution in Sodium Molybdate at 974 K and Enthalpies of Formation from the Oxides and from the Elements at 298 K for $NaTi_xNb_{1-x}O_{3-0.5x}$ Perovskites

x	ΔH_{ds} (kJ/mol)[a]	$\Delta H_{f,ox}°$ (kJ/mol)	$\Delta H_{f,el}°$ (kJ/mol)
0	94.6 ± 0.5 (12)	−157.4 ± 2.2	−1314.6 ± 3.1
0.05	94.0 ± 0.5 (7)	−156.2 ± 2.2	−1313.0 ± 3.0
0.1	92.3 ± 0.4 (6)	−153.8 ± 2.2	−1310.4 ± 2.9
0.15	90.1 ± 0.4 (6)	−151.0 ± 2.2	−1307.3 ± 2.8
0.2	86.2 ± 0.5 (5)	−146.5 ± 2.2	−1302.5 ± 2.8

[a] Uncertainty is two standard deviations of the mean; value in ( ) is the number of experiments.

Na_2O, Nb_2O_5, and TiO_2 (Table 4),[31−33] we calculated the standard molar enthalpies of formation of the perovskite phases from the constituent oxides ($\Delta H_{f,ox}°$) via the following thermochemical cycle:

$$(^1/_2)Na_2O\ (s, 298\ K) \rightarrow (^1/_2)Na_2O\ (soln, 974\ K) \quad (1)$$

$$xTiO_2\ (s, 298\ K) \rightarrow xTiO_2\ (soln, 974\ K) \quad (2)$$

$$(^1/_2 - {}^x/_2)Nb_2O_5\ (s, 298\ K) \rightarrow (^1/_2 - {}^x/_2)Nb_2O_5\ (soln, 974\ K) \quad (3)$$

$$(^1/_2)Na_2O\ (soln, 974\ K) + xTiO_2\ (soln, 974\ K) + (1/2 - x/2)Nb_2O_5\ (soln, 974\ K) \rightarrow NaTi_xNb_{1-x}O_{3-0.5x}\ (s, 298\ K) \quad (4)$$

$$(^1/_2)Na_2O\ (s, 298\ K) + xTiO_2\ (s, 298\ K) + (^1/_2 - {}^x/_2)Nb_2O_5\ (s, 298\ K) \rightarrow NaTi_xNb_{1-x}O_{3-0.5x}\ (s, 298\ K) \quad (5)$$

from which the enthalpies of formation of $NaTi_xNb_{1-x}O_{3-0.5x}$ perovskites are computed as follows: $\Delta H_{f,ox}° = \Delta H_1 + \Delta H_2 + \Delta H_3 + \Delta H_4$.

Similarly, the enthalpies of formation of these phases from the elements ($\Delta H_{f,el}°$) can be derived from their $\Delta H_{f,ox}°$ values and the $\Delta H_{f,el}°$ values of the constituent oxides (Table 4) by using an appropriate reaction cycle. The enthalpies of formation thus obtained are presented in Table 3. The only previously reported enthalpies of formation in this system are for the end-member $NaNbO_3$ ($\Delta H_{f,ox}° = -153.5 \pm 2.3$ kJ/mol; $\Delta H_{f,el}° = -1312.2 \pm 3.8$ kJ/mol),[32] and they are in good agreement with our values ($\Delta H_{f,ox}° = -157.4 \pm 2.2$ kJ/mol; $\Delta H_{f,el}° = -1314.6 \pm 3.1$ kJ/mol).

Figure 8B shows the enthalpies of formation of $NaTi_xNb_{1-x}O_{3-0.5x}$ perovskites from the oxides as a function of composition. As Ti content increases, $\Delta H_{f,ox}°$ becomes less exothermic. This behavior suggests a destabilizing effect of the charge-coupled substitution, $Ti^{4+} + 0.5V_O^{\bullet\bullet} \rightarrow Nb^{5+}$, on the perovskite structure with respect to the constituent oxides. However, as described earlier, the structures of Ti-substituted perovskites become less distorted (the tolerance factor t is closer to unity) with increasing Ti content. Previous thermochemical studies on various perovskites demonstrate

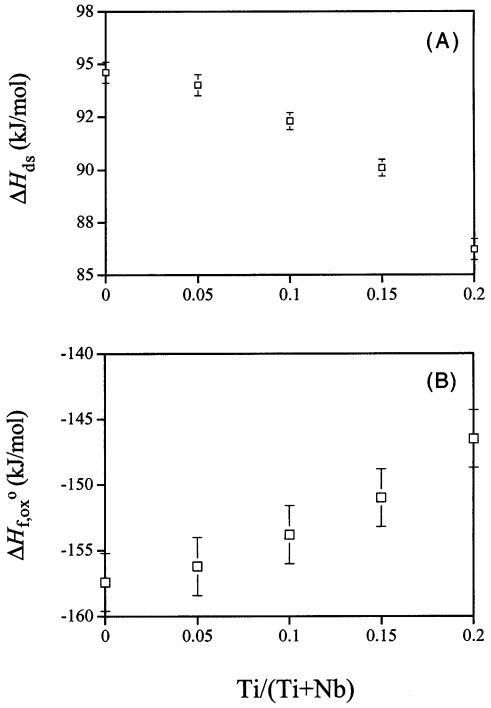

Figure 8. Variation of (A) the enthalpies of drop solution in sodium molybdate at 974 K and (B) the enthalpies of formation from the oxides at 298 K for $NaTi_xNb_{1-x}O_{3-0.5x}$ perovskites as a function of composition.

Table 4. Enthalpies of Drop Solution in Sodium Molybdate at 974 K and Enthalpies of Formation from the Elements at 298 K of Several Oxides Used in Calculations of the Enthalpies of Formation of $NaTi_xNb_{1-x}O_{3-0.5x}$ Perovskites

oxide	Na_2O	Nb_2O_5	TiO_2
ΔH_{ds} (kJ/mol)	−217.56 ± 4.25[a]	91.97 ± 0.78[b]	58.73 ± 0.91[c]
$\Delta H_{f,el}°$ (kJ/mol)	−414.8 ± 0.3[d]	−1899.54 ± 4.2[e]	−944.0 ± 0.8[d]

[a] From ref 31. [b] From ref 32. [c] From ref 33. [d] From ref 34. [e] From ref 35.

that the less the tolerance factor t deviates from unity, the more negative the enthalpy of formation.[36] This discrepancy implies that other structural factors must cause the destabilization of Ti-substituted perovskites, and further, they play a dominant role in the energetics of this solid solution series. One probable factor is the creation of O^{2-} vacancies, needed for compensating the charge imbalance between Ti^{4+} and Nb^{5+}, in the structure. Because [BO_6] octahedra are linked through corner-sharing oxygens into a three-dimensional framework, the occurrence of O^{2-} vacancies disrupts the continuity of the framework, thereby destabilizing the structure. Another factor is the size mismatch between the substituting Nb^{5+} and Ti^{4+}, which results in increased strain energy as Ti content increases. Similar behavior has been observed in other solid solution series

(31) Tessier, F.; Navrotsky, A.; Le Sauze, A.; Marchand, R. *Chem. Mater.* **2000**, *12*, 148.
(32) Pozdnyakova, I.; Navrotsky, A.; Shilkina, L.; Reznichenko, L. *J. Am. Ceram. Soc.* **2002**, *85*, 379.
(33) Putnam, R. L.; Navrotsky, A.; Woodfield, B. F.; Boerio-Goates, J.; Shapiro, J. L. *J. Chem. Thermodyn.* **1999**, *31*, 229.
(34) Robie, R. A.; Hemingway, B. S. *Thermodynamic Properties of Minerals and Related Substances at 298.15 K and 1 Bar (105 Pascals) Pressure and at Higher Temperatures*; Geological Survey Bulletin No. 2131; United States Government Printing Office: Washington, DC, 1995.
(35) Chase, M. W. *NIST-JANAF Thermochemical Tables*, 4th ed.; Journal of Physical and Chemical Reference Data, No. 9; American Chemical Society: Washington, DC; AIP/NIST: Woodbury, NY, 1998.
(36) Navrotsky, A. In *Fundamental Physics of Ferroelectrics 2000: Aspen Center for Physics Workshop*; Cohen, R. E., Ed.; American Institute of Physics: Woodbury, NY, 2000; pp 288−296.

such as $CsTi_xAl_{1-x}Si_2O_{6+0.5x}$ pollucites.[37] Last, as described above, Nb^{5+} and Ti^{4+} in $NaTi_xNb_{1-x}O_{3-0.5x}$ perovskites are ordered on short-range scales, and their locations are strongly correlated with those of the concomitant O vacancies. The $[TiO_5]$ and $[NbO_6]$ coordination geometries require that Nb−O−Nb and Ti−O−Nb be the only two possible B−O−B linkages in the structure. Since O in Ti−O−Nb (net oxygen charge = −0.37) is more underbonded than O in Nb−O−Nb (net charge = −0.33), the Ti−O−Nb configuration may be energetically unfavorable relative to Nb−O−Nb. Hence, as Ti content increases, the amount of Ti−O−Nb increases, and the structure becomes destabilized.

Although the geometrical constraints for $[TiO_5]$ and $[NbO_6]$ dictate that the B−O−B linkages are limited to be Nb−O−Nb and Ti−O−Nb, there are more possible configurations for the next-nearest neighbors such as Ti−O−Nb−O−Nb−O−Ti and Nb−O−Nb−O−Nb−O−Ti. Moreover, unlike the B−O−B linkages whose constituents (ratio of Nb−O−Nb to Ti−O−Nb) solely depend on the sample composition, the components for B−O−B−O−B−O−B depend on not only the composition but also the synthesis conditions (such as heat-treatment temperature and time) as well. Though all of our $NaTi_xNb_{1-x}O_{3-0.5x}$ samples were crystallized from their gels at 1173 K for ∼15 h, since their crystallization kinetics probably vary with Ti content (our DTA measurements show that the crystallization temperatures of the gels increase with increasing Ti), their degrees of Nb/Ti short-range order are probably different. This may explain the small curvatures present in the variations of ΔH_{ds} and $\Delta H_{f,ox}°$ as a function of Ti/(Ti + Nb) (Figure 8A,B). More specifically, the degree of Nb/Ti ordering probably decreases with increasing Ti content, resulting in the increased destabilization in terms of the enthalpies as x increases. However, to further establish the relation between the state of Nb/Ti short-range order of Ti-substituted perovskites and their energetic behavior, ^{93}Nb NMR and Ti XAS measurements are needed.

(37) Xu, H.; Navrotsky, A.; Balmer, M. L.; Su, Y.; Bitten, E. R. *J. Am. Ceram. Soc.* **2001**, *84*, 555.

Conclusions

A series of perovskite solid solutions has been synthesized in the $NaTi_xNb_{1-x}O_{3-0.5x}$ ($0 \le x \le 0.2$) system using the sol−gel method. With increasing Ti content, the tolerance factor t of the substituted phases becomes closer to unity and thus the structure more cubiclike. Variation of the enthalpies of formation with composition suggests that the $Ti^{4+} + 0.5V_O^{\bullet\bullet} \rightarrow Nb^{5+}$ substitution destabilizes the perovskite structure. This behavior is attributed to several structural factors including the occurrence of O^{2-} vacancies and of Ti−O−Nb linkages as well as the size mismatch between Ti^{4+} and Nb^{5+}.

Acknowledgment. This work was supported by the U.S. Department of Energy (DOE) Environmental Management Science Program (EMSP) (Grant No. FG07-97ER45674). Neutron diffraction was performed at the Maneul Lujan, Jr. Neutron Scattering Center, Los Alamos National Laboratory (LANL), which is operated by the University of California for DOE. Sample synthesis and Raman spectroscopy were carried out at the Environmental Molecular Sciences Laboratory, a national scientific user facility sponsored by the DOE Office of Biological and Environmental Research and located at the Pacific Northwest National Laboratory (PNNL). PNNL is operated for DOE by Battelle Memorial Institute. We thank two anonymous reviewers for helpful comments, P. Encinias for assistance with the neutron experiments, J. Shackelford for financial support for a trip to LANL (H.X.) through the HIPPO beamline fund, and T. Nenoff and M. Nyman for discussions.

CM020963S